The current issue and full text archive of this journal is available at
www.emeraldinsight.com/0264-4401.htm

Received 12 August 2008
Revised 17 November 2008
Accepted 15 December 2008

Analytical trial function method for development of new 8-node plane element based on the variational principle containing Airy stress function

Xiang-Rong Fu
Department of Engineering Mechanics, School of Aerospace, Tsinghua University, Beijing, China, and College of Water Conservancy and Civil Engineering, China Agriculture University, Beijing, China
Song Cen
Department of Engineering Mechanics, School of Aerospace, Tsinghua University, Beijing, China, and Failure Mechanics Laboratory, Tsinghua University, Beijing, China
C.F. Li
Civil and Computational Engineering Centre, School of Engineering, Swansea University, Swansea, UK, and
Xiao-Ming Chen
Department of Engineering Mechanics, School of Aerospace, Tsinghua University, Beijing, China, and Institute of Building Structures, China Academy of Building Research, Beijing, China

Abstract

Purpose – The purpose of this paper is to propose a novel and simple strategy for construction of hybrid-"stress function" plane element.

Design/methodology/approach – First, a complementary energy functional, in which the Airy stress function is taken as the functional variable, is established within an element for analysis of plane problems. Second, 15 basic analytical solutions (in global Cartesian coordinates) of the stress function are taken as the trial functions for an 8-node element, and meanwhile, 15 unknown constants are then introduced. Third, according to the principle of minimum complementary energy, the unknown constants can be expressed in terms of the displacements along element edges, which are interpolated by element nodal displacements. Finally, the whole system can be rewritten in terms of element nodal displacement vector.

Findings – A new hybrid element stiffness matrix is obtained. The resulting 8-node plane element, denoted as analytical trial function (ATF-Q8), possesses excellent performance in numerical examples. Furthermore, some numerical defects, such as direction dependence and interpolation failure, are not found in present model.

Originality/value – This paper presents a new strategy for developing finite element models exhibits advantages of both analytical and discrete method.

Keywords Finite element analysis, Stress, Functional analysis, Modelling, Variational techniques

Paper type Research paper

Engineering Computations: International Journal for Computer-Aided Engineering and Software
Vol. 27 No. 4, 2010
pp. 442-463

0264-4401
DOI 10.1108/02644401011044568

This study was supported by the Natural Science Foundation of China (Project No. 10872108), the Special Foundation for the Authors of the Nationwide (China) Excellent Doctoral Dissertation (Project No. 200242), the Programme for New Century Excellent Talents in University (Project No. NCET-07-0477), and the Erasmus Mundus Scholarship.

1. Introduction

As a model with quadric interpolation functions in isoparametric coordinates, the standard 8-node isoparametric element (Q8) is one of the most commonly used finite element models in scientific and engineering computations. Its performance has been thoroughly assessed by researchers in early time. Stricklin *et al.* (1977) presented some results for a cantilever beam modelled using distorted and undistorted elements, and they showed that Q8 element stiffened and performed very badly when it was distorted. Lee and Bathe (1993) studied the various influences to some Serendipity (Q8, Q12) and Lagrangian (Q9, Q16) elements using various distorted meshes. They pointed out that the displacement fields of Q8 and Q12 are only C^1 completeness in Cartesian coordinates under distorted conditions, while Q9 and Q16 could reach much higher order of completeness. Therefore, the Lagrangian type elements process better stability in most cases, and were strongly recommended. Zienkiewicz and Taylor (1989) have made the same conclusion. Unfortunately, Lagrangian elements usually contain internal nodes so that their formulations are more complicated than those of the corresponding Serendipity elements. Thus, the latter is still preferred in many practical applications.

During the past ten years, some researchers have made great efforts on developments of new 8-node plane elements with improved performance. Kikuchi *et al.* (1999) proposed a modified 8-node Serendipity model by defining a basic principle of constructing 8-D spaces including the Cartesian quadratic polynomial space when the quadrilateral is of bilinear isoparametric shape. Although this element performs better than original Q8 element, it still cannot well represent the behaviours of the Cartesian quadratic polynomials in the fully isoparametric cases. Li *et al.* (2004) followed the frame of Kikuchi *et al.* (1999) and proposed a new Q8α element. It has the same performance as that of the model in Kikuchi *et al.* (1999), but possesses simpler formulations. In 2003, Rajendran and Liew (2003) used two different sets of shape functions (metric set and isoparametric set) as the trial and test functions, respectively, and constructed an 8-node element, US-QUAD8, with unsymmetric element stiffness matrix. This US-QUAD8 element exhibits excellent performance for several benchmark problems and is immune to various mesh distortion. However, the use of metric shape functions as trial functions causes the element to exhibit rotational frame dependence as well as interpolation failure under certain conditions (Ooi *et al.*, 2008). By employing bivariate quadratic splines on triangulated quadrangulations, Li and Wang (2006) proposed a new 8-node spline element L8 in 2006. Good results for some problems can be obtained after a relatively complicated mathematical treatment. At the end of last century, Long *et al.* (1999a, b) established a new natural coordinate system, the quadrilateral area coordinate method, for constructions of quadrilateral finite element model. On the basis of the new tool, three 8-node models, AQ8-I, AQ8-II and QACM8, were successfully developed by Soh *et al.* (2000) and Cen *et al.* (2007), respectively. When all element edges are straight, the interpolation functions for the displacement fields of these elements will possess second-order completeness in both area and Cartesian coordinates, so all the elements can exhibit excellent performance in bending problems, and are insensitive to mesh distortion. However, once any element edge is curved, the above second-order completeness will no longer exist.

Variational principles are usually considered as the theoretical basis of the finite element method. Washizu (1982), Chien (1980), Hu (1984) have presented systematical discussions on this topic. The principles of minimum potential energy and complementary energy are both the classical single-field variational principles, and contain only single type of functional variables (displacement or stress, respectively).

The Hellinger-Reissner principle is the classical two-field variational principle and contains two types of functional variables (both displacement and stress). The Hu-Washizu principle is the classical three-field variational principle and contains three types of functional variables (displacement, strain and stress). On the basis of these various variational principles, finite element models with different characters can be derived, such as the displacement-based element, the stress-based element, the hybrid element, the mixed element, and so on. Those functional variables, which are also the variables in the governing equations of elasticity, will be finally solved. Meanwhile, it is known that the stress function can also be treated as the unknown variable for solving plane elastic problem. However, it has been ignored in most variational principles for a long time and seldom taken as the functional variable.

In this paper, a novel and simple strategy for construction of hybrid-"stress function" plane element is proposed for the first time. First, a complementary energy functional, in which the Airy stress function φ is taken as the functional variable, is established within an element for analysis of plane problems. Second, 15 basic analytical solutions (in global Cartesian coordinates) of φ are taken as the trial functions for an 8-node element, and meanwhile, 15 unknown constants are then introduced. Third, according to the principle of minimum complementary energy, the unknown constants can be expressed in terms of the displacements along element edges, which are interpolated by element nodal displacements. Finally, the whole system can be rewritten in terms of element nodal displacement vector, and thus, a new hybrid element stiffness matrix is obtained. The resulting 8-node plane element, denoted as analytical trial function (ATF-Q8), possesses excellent performance in all numerical examples. Furthermore, some numerical defects, such as direction dependence and interpolation failure, are not found in present model.

2. Element complementary energy functional containing the Airy stress function

For a plane finite element model, its complementary energy functional can be written in the following matrix form:

$$\Pi_C = \Pi_C^* + V_C^* = \frac{1}{2}\iint_{A^e} \boldsymbol{\sigma}^{\mathrm{T}}\mathbf{C}\boldsymbol{\sigma} t \mathrm{d}A - \int_{\Gamma} \mathbf{T}^{\mathrm{T}}\bar{\mathbf{u}} t \mathrm{d}s, \tag{1}$$

with

$$\Pi_C^* = \frac{1}{2}\iint_{A^e} \boldsymbol{\sigma}^{\mathrm{T}}\mathbf{C}\boldsymbol{\sigma} t \mathrm{d}A, \quad V_C^* = -\int_{\Gamma} \mathbf{T}^{\mathrm{T}}\bar{\mathbf{u}} t \mathrm{d}s, \tag{2}$$

$$\boldsymbol{\sigma} = \begin{Bmatrix} \sigma_x \\ \sigma_y \\ \tau_{xy} \end{Bmatrix}, \quad \mathbf{C} = \frac{1}{E'}\begin{bmatrix} 1 & -\mu' & 0 \\ -\mu' & 1 & 0 \\ 0 & 0 & 2(1+\mu') \end{bmatrix}, \quad \mathbf{T} = \begin{Bmatrix} T_x \\ T_y \end{Bmatrix}, \quad \bar{\mathbf{u}} = \begin{Bmatrix} \bar{u} \\ \bar{v} \end{Bmatrix}, \tag{3}$$

where Π_C^* is the complementary energy within the element; V_C^* is the complementary energy along the element boundaries; t is the thickness of the element; $\boldsymbol{\sigma}$ is the element stress vector; $\mathbf{T}$ is the surface force vector along the element boundaries; $\bar{\mathbf{u}}$ is the displacement vector along element boundaries; $\mathbf{C}$ is the elastic flexibility matrix; in which $E' = E$ and $\mu' = \mu$ for plane stress problem, and $E' = E/(1-\mu^2)$ and $\mu' = \mu/(1-\mu)$ for plane strain problem. E and μ are Young's modulus and Poisson's ratio, respectively.

After introducing the Airy stress function φ, the stress vector $\boldsymbol{\sigma}$ can be expressed by:

$$\boldsymbol{\sigma} = \begin{Bmatrix} \sigma_x \\ \sigma_y \\ \tau_{xy} \end{Bmatrix} = \begin{Bmatrix} \dfrac{\partial^2 \varphi}{\partial y^2} \\ \dfrac{\partial^2 \varphi}{\partial x^2} \\ -\dfrac{\partial^2 \varphi}{\partial x \partial y} \end{Bmatrix} = \tilde{\mathbf{R}}(\varphi); \tag{4}$$

and the surface force vector $\mathbf{T}$ can be written as:

$$\mathbf{T} = \begin{Bmatrix} T_x \\ T_y \end{Bmatrix} = \begin{bmatrix} l & 0 & m \\ 0 & m & l \end{bmatrix} \begin{Bmatrix} \sigma_x \\ \sigma_y \\ \tau_{xy} \end{Bmatrix} = \mathbf{L}\tilde{\mathbf{R}}(\varphi) \quad \text{with} \quad \mathbf{L} = \begin{bmatrix} l & 0 & m \\ 0 & m & l \end{bmatrix}, \tag{5}$$

where l and m are the direction cosines of the outer normal n of the element boundaries.

Substitution Equations (4) and (5) into Equation (1) yields:

$$\Pi_C = \Pi_C^* + V_C^* = \frac{1}{2}\iint_{A^e} \tilde{\mathbf{R}}(\varphi)^{\mathrm{T}} \mathbf{C} \tilde{\mathbf{R}}(\varphi) t \mathrm{d}A - \int_{\Gamma} [\mathbf{L}\tilde{\mathbf{R}}(\varphi)]^{\mathrm{T}} \bar{\mathbf{u}} t \mathrm{d}s, \tag{6}$$

where

$$\Pi_C^* = \frac{1}{2}\iint_{A^e} \tilde{\mathbf{R}}(\varphi)^{\mathrm{T}} \mathbf{C} \mathbf{R}(\varphi) t \mathrm{d}A, \tag{7}$$

$$V_C^* = -\int_{\Gamma} [\mathbf{L}\mathbf{R}(\varphi)]^{\mathrm{T}} \bar{\mathbf{u}} t \mathrm{d}s. \tag{8}$$

Thus, the element complementary energy functional containing the Airy stress function is established.

3. Analytical solutions of the stress function

In a plane problem without body forces, the Airy stress function φ should satisfy the following biharmonic equation:

$$\nabla^4 \varphi = \frac{\partial^4 \varphi}{\partial x^4} + 2\frac{\partial^4 \varphi}{\partial x^2 \partial y^2} + \frac{\partial^4 \varphi}{\partial y^4} = 0. \tag{9}$$

If a polynomial in Cartesian coordinates satisfies Equation (9), it can be treated as the basic analytical solution of stress function φ. Actually, there are numerous polynomials that can satisfy Equation (9). In order to choose appropriate solutions as the trial functions for the construction of new element model, two principles must be followed:

(1) The basic analytical solutions of stress function φ should be selected in turn from the lowest-order to higher-order.

(2) The resulting stress fields should possess completeness in Cartesian coordinates.

Here, 15 such solutions and resulting stresses are listed in Table I. Obviously, the stress fields composed of these stress solutions can reach three-order completeness in x and y.

4. Analytical trial function method for developing a new 8-node hybrid element

Consider the 8-node quadrilateral element shown in Figure 1, any edge of the element can be either straight or curved, and the element nodal displacement vector $\mathbf{q}^e$ is given by

$$\mathbf{q}^e = [\,u_1 \quad v_1 \quad u_2 \quad v_2 \quad u_3 \quad v_3 \quad u_4 \quad v_4 \quad u_5 \quad v_5 \quad u_6 \quad v_6 \quad u_7 \quad v_7 \quad u_8 \quad v_8\,]^{\mathrm{T}}, \tag{10}$$

where u_i, and v_i (i = 1-8) are the nodal displacements in x- and y-directions, respectively.

Now, the 15 analytical solutions for the stress function, which have been listed in Table I, are taken as the trial function. Let:

i	1	2	3	4	5	6	7	8	9
φ_i	x^2	xy	y^2	x^3	$x^2\,y$	xy^2	y^3	$x^3\,y$	xy^3
σ_x	0	0	2	0	0	$2x$	$6y$	0	$6xy$
σ_y	2	0	0	$6x$	$2y$	0	0	$6xy$	0
τ_{xy}	0	-1	0	0	$-2x$	$-2y$	0	$-3x^2$	$-3y^2$

i	10	11	12	13	14	15
φ_i	x^4-y^4	$6x^2y^2-x^4-y^4$	$X^3y^2-xy^4$	$5x^3y^2-x^5$	$x^2y^3-x^4y$	$5x^2y^3-y^5$
σ_x	$-12y^2$	$12(x^2-y^2)$	$2x(x^2-6y^2)$	$10x^3$	$6x^2y$	$10y(3x^2-2y^2)$
σ_y	$12x^2$	$-12(x^2-y^2)$	$6xy^2$	$-10x(2x^2-3y^2)$	$-2y(6x^2-y^2)$	$10y^3$
τ_{xy}	0	$-24xy$	$-2y(3x^2-2y^2)$	$-30x^2y$	$2x(2x^2-3y^2)$	$-30xy^2$

Table I.
Fifteen basic analytical solutions of stress function and stresses for plane problem

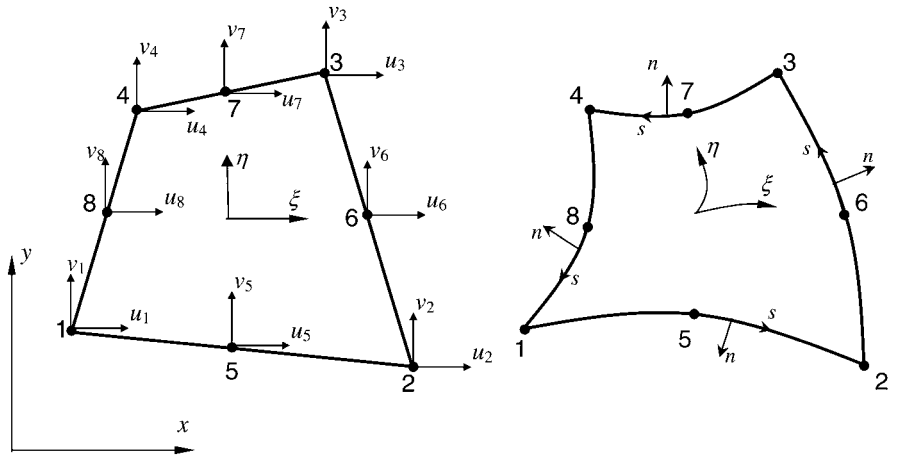

Figure 1.
An 8-node quadrilateral plane element

$$\varphi = \sum_{i=1}^{15} \varphi_i \beta_i = \boldsymbol{\varphi}\boldsymbol{\beta}, \tag{11}$$

with

$$\begin{aligned} \boldsymbol{\varphi} &= [\,\varphi_1 \quad \varphi_2 \quad \varphi_3 \quad \cdots \quad \cdots \quad \varphi_{15}\,] \\ \boldsymbol{\beta} &= [\,\beta_1 \quad \beta_2 \quad \beta_3 \quad \cdots \quad \cdots \quad \beta_{15}\,]^{\mathrm{T}}, \end{aligned} \tag{12}$$

where φ_i (i = 1-15) are the 15 analytical solutions for stress function; β_i (i = 1-15) are 15 unknown constants.

Substitution of Equation (11) into Equation (7) yields:

$$\Pi_C^* = \frac{1}{2}\boldsymbol{\beta}^{\mathrm{T}}\mathbf{M}\boldsymbol{\beta}, \tag{13}$$

with

$$\mathbf{M} = \iint_{A^e} \mathbf{S}^{\mathrm{T}}\mathbf{C}\mathbf{S}t\mathrm{d}A, \tag{14}$$

where the expression of matrix $\mathbf{S}$ and the evaluation procedure of symmetrical matrix $\mathbf{M}$ are given in the Appendix.

Substitution of Equation (11) into Equation (8) yields:

$$V_C^* = -\boldsymbol{\beta}^{\mathrm{T}}\mathbf{H}\mathbf{q}^e, \tag{15}$$

with

$$\mathbf{H} = \int_{\Gamma} \mathbf{S}^{\mathrm{T}}\mathbf{L}^{\mathrm{T}}\overline{\mathbf{N}}t\mathrm{d}s, \tag{16}$$

where the expression of matrix $\overline{\mathbf{N}}$ and the evaluation procedure of matrix $\mathbf{H}$ are also given in the Appendix.

Then, after substituting Equations (13) and (15) into Equation (6), the element complementary energy functional can be rewritten as:

$$\Pi_C = \frac{1}{2}\boldsymbol{\beta}^{\mathrm{T}}\mathbf{M}\boldsymbol{\beta} - \boldsymbol{\beta}^{T}\mathbf{H}\mathbf{q}^e. \tag{17}$$

According to the principle of minimum complementary energy, we have:

$$\frac{\partial \Pi_C}{\partial \boldsymbol{\beta}} = \mathbf{0}. \tag{18}$$

Thus, by substituting Equation (17) into Equation (18), the unknown constant vector $\boldsymbol{\beta}$ can be expressed in terms of the nodal displacement vector $\mathbf{q}^e$:

$$\boldsymbol{\beta} = \mathbf{M}^{-1}\mathbf{H}\mathbf{q}^e. \tag{19}$$

Substitution of Equation (19) into Equation (13) yields:

$$\Pi_C^* = \frac{1}{2}\mathbf{q}^{e^T}\mathbf{K}^*\mathbf{q}^e, \tag{20}$$

where

$$\mathbf{K}^* = (\mathbf{M}^{-1}\mathbf{H})^{\mathrm{T}}\mathbf{H}. \tag{21}$$

From the viewpoint of the hybrid-stress element, matrix $\mathbf{K}^*$ in the above equation can be considered as the stiffness matrix of the new hybrid-"stress function" element, and therefore, it can be used in the conventional finite element equation.

Once the element nodal displacement vector $\mathbf{q}^e$ is solved, the element stresses can be given by:

$$\boldsymbol{\sigma} = \mathbf{S}\mathbf{M}^{-1}\mathbf{H}\mathbf{q}^e. \tag{22}$$

The stress solution at any point can be readily obtained by substituting the Cartesian coordinates of this point within an element into $\mathbf{S}$ in the above equation.

The determination procedure of the nodal equivalent load is the same as that of the conventional 8-node isoparametric element Q8.

Thus, a new 8-node quadrilateral plane element is formulated, and this new element is named ATF-Q8 in this paper.

5. Numerical examples

Ten different problems are used to evaluate and test the performance of the new element ATF-Q8, and the results obtained by ten different 8-node plane element models, as listed below, are also given for comparison.

- *Q8, Q9, Q12:* conventional 8-node, 9-node and 12-node quadrilateral isoparametric elements;
- *Q8/9:* improved 8-node isoparametric element from 9-node model, Kikuchi *et al.* (1999);
- *Q8α:* improved 8-node isoparametric element from 9-node model, Li *et al.* (2004);
- *L8:* 8-node quadrilateral spline finite element, Li and Wang (2006);
- *US-QUAD8:* 8-node element with unsymmetric element stiffness matrix, Rajendran and Liew (2003), Ooi *et al.* (2008);
- *AQ8-I and II:* 8-node elements formulated by the quadrilateral area coordinate method, Soh *et al.* (2000); and
- *QACM8:* 8-node element formulated by the quadrilateral area coordinate method, Cen *et al.* (2007).

These models are all displacement-based elements. So, some element stiffness matrices of them can be evaluated by the reduced integration scheme which can soften element stiffness and bring better displacement solutions in many occasions. However, there are still some technical problems when using the reduced integration scheme, such as hourglass phenomenon and incorrect stress solutions (although the displacement

solutions are exact). Therefore, in this paper, only the full integration scheme is considered for all above elements since it possesses strict theoretical base.

The stress solutions at any point within an ATF-Q8 element can be directly evaluated by Equation (22). Since the stress fields of the present element ATF-Q8 reach third-order completeness in Cartesian coordinates (see Table I), the stress solutions may possess high accuracy.

Furthermore, some numerical defects, as described in Ooi *et al.* (2008), are not found in this novel hybrid-"stress function" model.

5.1 Some traditional benchmark examples

Example 1: Constant stress/stress patch test. A small patch is divided into some arbitrary elements, as shown in Figure 2. The displacement fields corresponding to the constant strain are:

$$u = 10^{-3}((x+y)/2), \quad v = 10^{-3}((y+x)/2)\,. \tag{23}$$

The exact stress solution is as follows:

$$\sigma_x = \sigma_y = 1333.3333, \quad \tau_{xy} = 400.0\,. \tag{24}$$

The coordinates and the displacement of control nodes are shown in Table II.

The displacements of the boundary nodes (5-12), as shown in Table II, are the displacement boundary conditions. No matter the inner element edges are straight or curved, the exact results of the displacements and stresses at each node can be obtained using the ATF-Q8 element. This demonstrates that the new elements pass the patch test and are able to ensure convergence. All conventional isoparametric elements also pass this patch test, while the quadrilateral area coordinate elements fail once any element edge is curved.

Example 2: Cantilever beam divided by five quadrilateral elements (Figure 3). The cantilever beam, as shown in Figure 3, is divided by five irregular quadrilateral elements. And two loading cases are considered:

(1) pure bending under moment M; and

(2) linear bending under transverse force P.

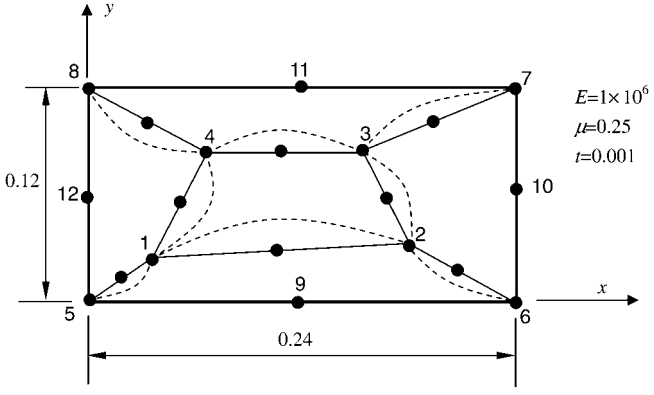

Figure 2.
Constant stress/strain patch test

Table II.
The coordinates and displacements ($\times 10^{-3}$) of control nodes in patch test (Figure 2)

Nodes	Coordinates		Displacements ($\times 10^{-3}$)	
	x_i	y_i	u_i	v_i
1	0.04	0.02	0.05	0.04
2	0.18	0.03	0.195	0.12
3	0.16	0.08	0.20	0.16
4	0.08	0.08	0.12	0.12
5	0.00	0.00	0.00	0.00
6	0.24	0.00	0.24	0.12
7	0.24	0.12	0.30	0.24
8	0.00	0.12	0.06	0.12
9	0.12	0.00	0.12	0.06
10	0.24	0.06	0.27	0.18
11	0.12	0.12	0.18	0.18
12	0.00	0.06	0.03	0.06

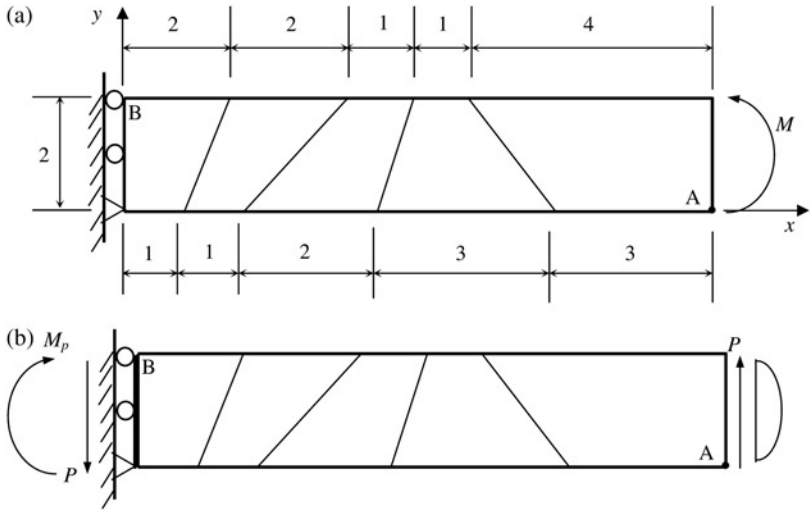

Notes: Pure bending M = 2,000, distributed as $f_x = -120y + 120$ and (b) linear bending P = 300, distributed as $f_y = 75y - 37.5y^2$; Mp = 3,000, distributed as $f_x = -180y + 180$

Figure 3.
Cantilever beam with five irregular elements

The Young's modulus $E = 1{,}500$, Poisson's ratio $\mu = 0.25$, thickness $t = 1.0$. The results of the vertical deflection v_A at point A and the stress σ_{xB} at point B are given in Table III.

Compared with the results given by other element models, it can be seen that the element ATF-Q8 presents the best answers. Exact solutions can be obtained by ATF-Q8 for the pure bending case.

Example 3: Cantilever beam divided by four quadrilateral elements (Figure 4). The cantilever beam is meshed into four irregular quadrilateral elements. The results of the deflections at tip points A, B and C are listed in Table IV. From Table IV, it can be seen again that the ATF-Q8 element is more precise than the other elements.

Example 4: Cook's skew beam problem (Figure 5). The skew cantilever under shear distributed load at the free edge was proposed by Cook (1989). The results of vertical deflection at point C, the maximum principal stress at point A and the minimum principal stress at point B are all listed in Table V. Compared with the other elements, the ATF-Q8 element exhibits the best convergence.

Example 5: MacNeal's thin cantilever beam with distorted meshes (Figure 6). Consider the thin beams presented in Figure 6. Three different mesh shapes are adopted: rectangular, parallelogram and trapezoidal. This example, proposed by MacNeal and Harder (1985), is a classic benchmark for testing the sensitivity to mesh distortion of the four-node quadrilateral membrane elements. Besides the distortion caused by the length-width ratio, the composite distortions of parallelogram and trapezoidal shapes together with length-width ratio are also taken into account.

There are two loading cases under consideration: pure bending and transverse linear bending. The Young's modulus of the beam is $E = 10^7$; the Poisson's ratio is $\mu = 0.3$; and the thickness of the beam is $t = 0.1$. The results of the tip deflection are shown

Elements	Load M		Load P	
	v_A	σ_{xB}	v_A	σ_{xB}
Q8	99.7	−2,984	101.5	−4,422
QACM8	101.3	−2,920	102.8	−4,320
ATF-Q8	*100.0*	*−3,000*	*102.6*	*−4,442*
Exact	100.0	−3,000	102.6	−4,500

Table III. The deflections and stresses at selected locations for bending problems of a cantilever beam (Figure 3)

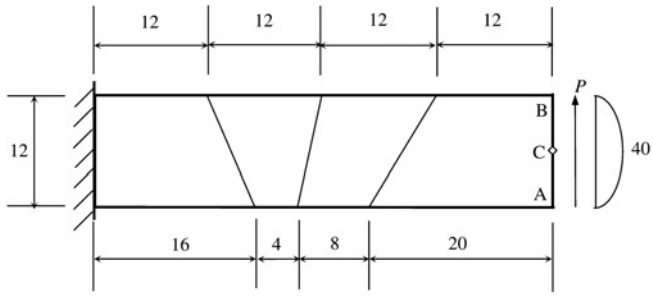

Notes: $E = 30{,}000.0$; $\mu = 0.25$; $t = 1.0$; $P = 40$, distributed as $f_y = 5y/3 - 5y^2/36$

Figure 4. Cantilever beam with four irregular elements

Element	Tip deflections				Normalized values			
	Point A	Point B	Point C	Average	Point A	Point B	Point C	Average
Q8	0.3481	0.3474	0.3481	0.3479	0.978	0.976	0.978	0.977
QACM8	0.3524	0.3517	0.3519	0.3520	0.990	0.988	0.989	0.989
ATF-Q8	0.3567	0.3561	*0.3558*	0.3562	1.003	1.001	*1.000*	1.001
Reference value at point C[a]			0.3558				1.000	

Source: [a]Long and XU (1994)

Table IV. The deflections at selected locations for bending problem of a cantilever beam (Figure 4)

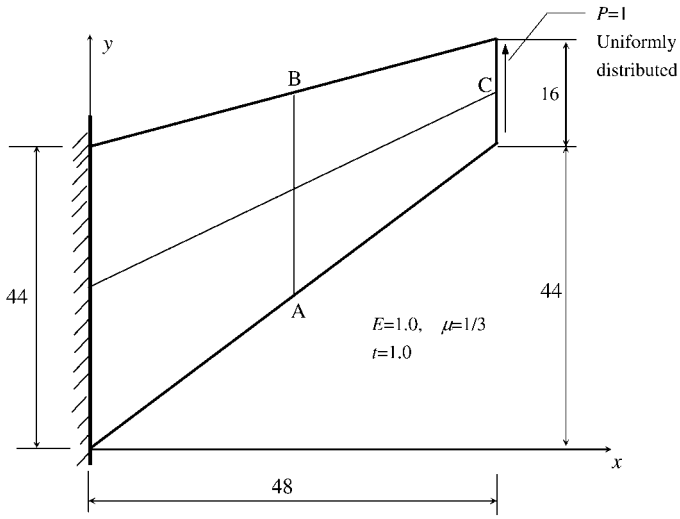

Figure 5.
Cook's skew beam problem

Element	v_C 2 × 2	4 × 4	8 × 8	σ_{Amax} 2 × 2	4 × 4	8 × 8	σ_{Bmin} 2 × 2	4 × 4	8 × 8
Q8	22.72	23.71	23.88	0.2479	0.2421	0.2390	−0.2275	−0.2007	−0.2041
Q9	23.29	23.84	23.94	–	–	–	–	–	–
Q8α	22.98	23.74	23.89	–	–	–	–	–	–
AQ8-I/II	22.98	23.74	23.89	0.2523	0.2415	0.2389	−0.2144	*−0.2024*	−0.2041
QACM8	22.98	23.74	23.89	0.1959	0.2414	0.2389	*−0.2142*	*−0.2024*	−0.2041
ATF-Q8	*23.80*	*23.96*	*23.96*	*0.2434*	*0.2404*	*0.2373*	−0.1771	−0.2049	*−0.2037*
Reference solution[a,b]		23.96			0.2362			– 0.2023	

Table V.
Results of Cook's skew beam (Figure 5)

Note: [a]Results of the element GT9M8
Source: [b]Long and Xu (1994) using 64 × 64 mesh

in Table VI. Besides the new elements, the results obtained by the other element models are also given for comparison. It can be seen that the proposed elements possesses high accuracy for all three mesh divisions, and are insensitive to these three types of distortion. Again, they can even provide the exact solutions for the pure bending problem.

Example 6: Thick curving beam (Figure 7). The thick curving cantilever beam meshed into four elements is subjected to a transverse force at its tip. The results of the vertical tip deflection at pint A are shown in Table VII. Much better and more stable solutions can be obtained by the present element than those by the other models.

Example 7: Thin curving beam (Figure 8). As shown in Figure 8, a thin curving cantilever beam is subjected to a transverse force P at the tip. Two mesh division types are employed:

(1) elements with curved edges; and

(2) elements with straight edges.

The results of the tip displacement are listed in Table VIII.

Compared with the mesh used in the Example 6, the shape of the elements in this example becomes much narrower. So the distortion becomes much more serious. From Table VIII, it can be observed that the new element possesses the best convergence.

5.2 The sensitive test for different mesh distortion

Example 8: Cantilever beam divided by two elements containing a parameter of distortion (Figure 9). The cantilever beam shown in Figure 9 is divided by two

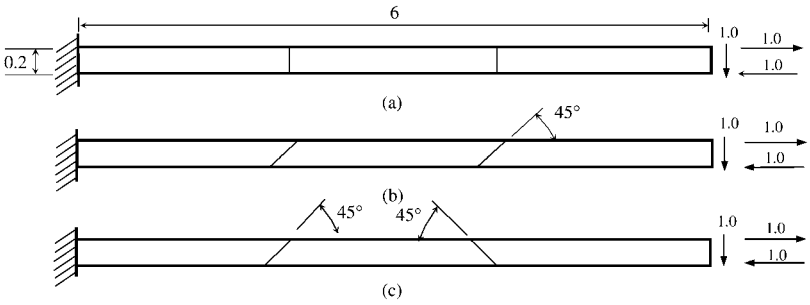

Figure 6.
MacNeal's beam problem

Element	Load P Mesh (a)	Mesh (b)	Mesh (c)	Load M Mesh (a)	Mesh (b)	Mesh (c)
Q8	0.951	0.919	0.854	*1.000*	0.994	0.939
QACM8	0.951	0.903	0.895	*1.000*	*1.000*	*1.000*
ATF-Q8	*0.978*	*0.968*	*0.966*	*1.000*	*1.000*	*1.000*
Exact		1.000[a]			1.000[b]	

Notes: [a]The standard value is −0.1081; [b]the standard value is −0.0054

Table VI.
The normalized results of the tip deflection for the MacNeal's thin beam using different meshes (Figure 6)

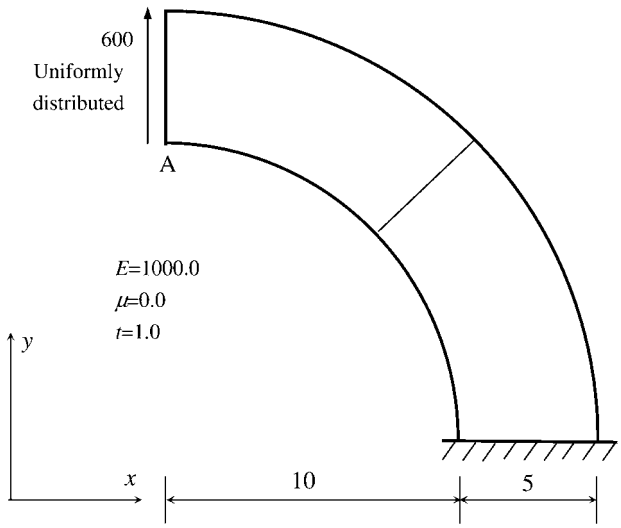

Figure 7.
Bending of a thick curving beam

elements. The shape of the two elements varies with the variety of the distorted parameter e and two distortion modes are considered. When $e = 0$, both elements are rectangular. But with the increase of e, the mesh will be distorted more and more seriously. This is another frequently used benchmark for testing the sensitivity to the mesh distortion. Two load cases:

(1) pure bending $M = 2{,}000$; and

(2) linear bending $P = 150$ are considered.

The results of the tip deflection at point A and the stress σ_x at point B are listed in Tables IX-XII.

Numerical results in Table IX show that the element ATF-Q8 can keep providing exact solutions for pure bending problem, that is to say, it is quite insensitive to mesh distortion mode I in a pure bending problem. But as to mesh distortion mode II, the element ATF-Q8 performs not so well as it in the previous test (see Table X). It seems that the element QACM8 provides the best answers for this case. But we should note

Table VII.
The tip deflection of a thick curving beam (Figure 7)

Elements	1×1	1×2	1×4	Exact solution
Q8	30.2	77.4	88.6	
QACM8	42.7	75.5	84.1	90.1
ATF-Q8	*56.5*	*90.5*	*90.4*	

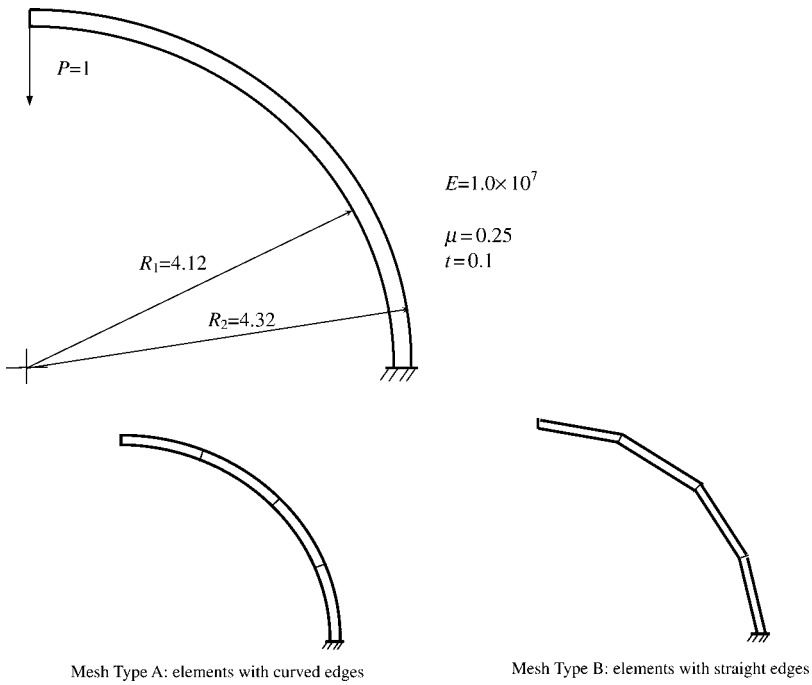

Figure 8.
Bending of a thin curving beam

Mesh	Q8	Q8/9	Q9	US-QUAD8	ATF-Q8	Exact solution
Mesh type A						
1 × 2	0.0888	0.0886	0.0890	0.0905	*0.1191*	
1 × 3	0.3132	0.3127	0.3143	*1.2485*	0.3812	
1 × 4	0.5817	0.5809	0.5840	*0.8397*	0.6512	
1 × 5	0.7672	0.7666	0.7702	*0.8494*	0.8232	1.000[a]
1 × 6	0.8688	0.8684	0.8718	0.8957	*0.9105*	
1 × 10	0.9769	0.9768	0.9790	0.9799	*0.9910*	
1 × 20	0.9963	0.9963	0.9974	0.9964	*0.9989*	
Mesh type B						
1 × 2	0.9288	–	0.9614	–	*1.054*	
1 × 3	0.9644	–	0.9788	–	*1.022*	
1 × 4	0.9785	–	0.9868	–	*1.012*	
1 × 5	0.9850	–	0.9907	–	*1.007*	1.000[a]
1 × 6	0.9887	–	0.9930	–	*1.004*	
1 × 10	0.9944	–	0.9966	–	*1.001*	
1 × 20	0.9976	–	0.9987	–	*1.000*	

Note: [a]The standard value is −0.0886

Table VIII.
The tip deflection of a thin curving beam (Figure 8)

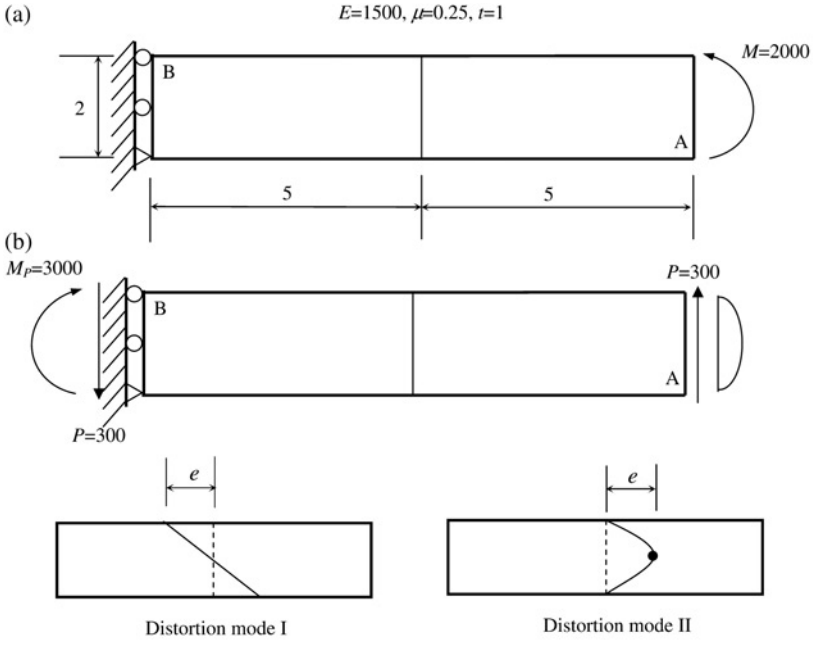

Notes: Pure bending $M = 2{,}000$, distributed as $f_x = -120y + 120$ and linear bending $P = 300$, distributed as $f_y = 75y - 37.5y^2$; Mp = 3,000, distributed as $f_x = -180y + 180$

Figure 9.
Cantilever beam divided by two element with distorted parameter *e*

that element QACM8 can not pass the constant stress/strain patch test once any element edge is curved, so its results given in Table X are not reliable.

From Tables XI and XII, it can be seen that the element ATF-Q8 can provide more stable answers for both mesh distortion modes in linear bending problem.

Example 9: Pure bending for a cantilever beam (Figure 10). This example is often used to test 8-node element models. As shown in Figure 10, seven meshes are used. The results listed in Table XIII show the element ATF-Q8 are relatively most insensitive to all kind of mesh distortion. So long as all element edges keep straight,

Table IX. Normalized results of the deflection and the stress at selected points of a cantilever beam subjected to a pure bending M: distortion mode I (Figure 9)

e	0	0.5	1	2	3	4	4.9
Deflection at point A, exact $v_A = 100.0$							
Q8	*1.000*	0.9996	0.9936	0.8939	0.5971	0.3201	0.1975
QACM8	*1.000*	*1.000*	1.002	1.007	1.019	1.037	1.059
ATF-Q8	*1.000*	*1.000*	*1.000*	*1.000*	*1.000*	*1.000*	*1.000*
Stress at point B, exact $\sigma_{xB} = -3{,}000$							
Q8	*1.000*	1.011	1.040	1.097	1.079	1.235	6.416
QACM8	*1.000*	0.9890	0.9677	0.9108	0.8665	0.8281	0.7793
ATF-Q8	*1.000*	*1.000*	*1.000*	*1.000*	*1.000*	*1.000*	*1.000*

Table X. Normalized results of the deflection and the stress at selected points of a cantilever beam subjected to a pure bending M: distortion mode II (Figure 9)

e	0	0.5	1	2	3	4	4.9
Deflection at point A, exact $v_A = 100$							
Q8	*1.000*	0.7448	0.4735	0.2486	0.1783	0.1457	0.1269
QACM8	*1.000*	0.9819	0.9667	*0.9450*	*0.9346*	*0.9364*	*0.9498*
ATF-Q8	*1.000*	*0.9943*	*0.9786*	0.9411	0.9163	0.9058	0.8991
Stress at point B, exact $\sigma_{xB} = -3{,}000$							
Q8	*1.000*	0.7000	0.4646	0.3402	0.3167	0.2998	0.2833
QACM8	*1.000*	*0.9624*	*0.9276*	*0.8653*	*0.8111*	*0.7635*	0.7254
ATF-Q8	*1.000*	0.8797	0.7750	0.6838	0.7008	0.7512	*0.7957*

Table XI. Normalized results of the deflection and the stress at selected points of a cantilever beam subjected to a linear bending P: distortion mode I (Figure 9)

e	0	0.5	1	2	3	4	4.9
Deflection at point A, exact $v_A = 102.6$							
Q8	0.9765	0.9630	0.9298	0.7992	0.5478	0.3255	0.2222
QACM8	0.9765	0.9698	0.9483	0.8830	0.8489	0.8421	*0.8470*
ATF-Q8	*0.9959*	*0.9919*	*0.9839*	*0.9697*	*0.9547*	*0.8946*	0.6916
Stress at point B, exact $\sigma_{xB} = -4{,}500$							
Q8	0.9152	0.9251	0.9257	0.9221	0.9486	1.216	7.188
QACM8	0.9152	0.9021	0.8585	0.7122	0.6120	0.5356	0.4681
ATF-Q8	*0.9468*	*0.9506*	*0.9521*	*0.9761*	*0.9860*	*0.9643*	*0.9321*

exact solutions can always be obtained by element ATF-Q8, no matter the meshes are distorted or not.

Example 10: Linear bending for a cantilever beam (Figure 11). The results of the deflection at selected point are listed in Table XIV. It is obvious that the ATF-Q8 element performs better than other 8-node element models.

e	0	0.5	1	2	3	4	4.9
Deflection at point A, exact $v_A = 102.6$							
Q8	0.9765	0.7677	0.5199	0.3064	0.2379	0.2040	0.1832
QACM8	0.9765	0.9493	0.9250	0.8850	0.8558	0.8382	0.8353
ATF-Q8	*0.9959*	*0.9953*	*0.9882*	*0.9696*	*0.9602*	*0.9596*	*0.9623*
Stress at point B, exact $\sigma_{xB} = -4{,}500$							
Q8	0.9152	0.6994	0.5088	0.3830	0.3417	0.3110	0.2854
QACM8	0.9152	0.8790	0.8456	0.7860	0.7344	0.6895	0.6537
ATF-Q8	*0.9468*	*0.9079*	*0.8758*	*0.8592*	*0.8848*	*0.9167*	*0.9404*

Table XII.
Normalized results of the deflection and the stress at selected points of a cantilever beam subjected to a linear bending P: distortion mode II (Figure 9)

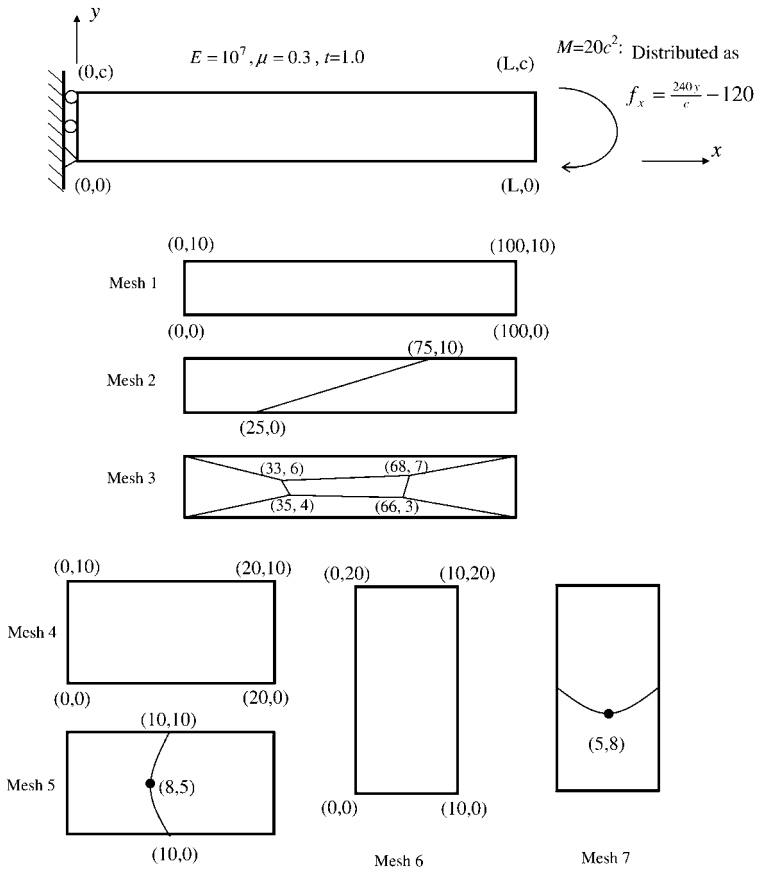

Figure 10.
Pure bending problem for a cantilever beam

	Q8	Q12	AQ8-I	QACM8	ATF-Q8	Exact
Mesh 1						
$\sigma_x(0,10)$	*120.000*	*120.0*	*120.000*	*120.000*	*120.000*	120.0
$\sigma_x(0,0)$	*−120.000*	*120.0*	*−120.000*	*−120.000*	*−120.000*	−120.0
$v(100,0) \times 10^3$	*−12.000*	*−12.00*	*−12.000*	*−12.000*	*−12.000*	−12.0
Mesh 2						
$\sigma_x(0,10)$	56.447	125.5	118.222	117.794	*120.000*	120.0
$\sigma_x(0,0)$	−74.863	−145.5	−114.667	−115.124	*−120.000*	−120.0
$v(100,0) \times 10^3$	−2.328	−5.18	−12.014	−12.046	*−12.000*	−12.0
Mesh 3						
$\sigma_x(0+,10)$	13.665	29.4	119.696	119.872	*120.000*	120.0
$\sigma_x(0,10-)$	5.262	14.0	118.887	119.327	*120.000*	120.0
$\sigma_x(0,0+)$	−5.665	−13.1	−119.112	−119.286	*−120.000*	−120.0
$\sigma_x(0+,0)$	−14.299	−28.5	−119.880	−119.816	*−120.000*	−120.0
$v(100,0) \times 10^3$	−0.477	−0.69	−11.997	−12.040	*−12.000*	−12.0
Mesh 4						
$\sigma_x(0,10)$	*120.000*	*120.000*	*120.000*	*120.000*	*120.000*	120.0
$\sigma_x(0,0)$	*−120.000*	*−120.000*	*−120.000*	*−120.000*	*−120.000*	−120.0
$v(20,0) \times 10^4$	*−4.800*	*−4.800*	*−4.800*	*−4.800*	*−4.800*	−4.8
Mesh 5						
$\sigma_x(0,10)$	*120.17*	120.9	130.39	130.39	123.49	120.0
$\sigma_x(0,0)$	*−120.17*	−120.9	−130.39	−130.39	−123.49	−120.0
$\sigma_x(10,10)$	99.389	–	120.77	120.77	*119.40*	120.0
$\sigma_x(10,0)$	−99.389	–	−120.77	−120.77	*−119.40*	−120.0
$v(20,0) \times 10^4$	−4.412	−4.774	−5.009	−5.009	*−4.810*	−4.8
Mesh 6						
$\sigma_x(0,20)$	*120.000*	*120.000*	*120.000*	*120.000*	*120.000*	120.0
$\sigma_x(0,0)$	*−120.000*	*−120.000*	*−120.000*	*−120.000*	*−120.000*	−120.0
$v(10,0) \times 10^5$	*−6.000*	*−6.000*	*−6.000*	*−6.000*	*−6.000*	−6.0
Mesh 7						
$\sigma_x(0,20)$	115.24	*120.3*	110.108	110.108	124.11	120.0
$\sigma_x(0,0)$	*−119.86*	−119.1	−133.611	−133.611	−114.97	−120.0
$\sigma_x(10,20)$	116.40	–	105.99	105.99	*120.05*	120.0
$\sigma_x(10,0)$	−118.59	–	−138.16	−138.16	*−120.69*	−120.0
$v(10,0) \times 10^5$	−6.045	*−5.994*	−6.546	−6.546	−6.063	−6.0

Table XIII.
Results of at selected locations for the pure bending problem (Figure 10)

6. Concluding remarks

In this paper, a novel strategy for developing new plane finite element method is proposed. The whole construction procedure is quite different with those of traditional models.

(1) First, a complementary energy functional, in which the Airy stress function φ is taken as the functional variable, is established within an element for analysis of plane problems.

(2) Second, 15 basic analytical solutions (in global Cartesian coordinates) of φ are taken as the trial functions for an 8-node element, and meanwhile, 15 unknown constants are then introduced.

(3) Third, according to the principle of minimum complementary energy, the unknown constants can be expressed in terms of the displacements along element edges, which are interpolated by element nodal displacements.

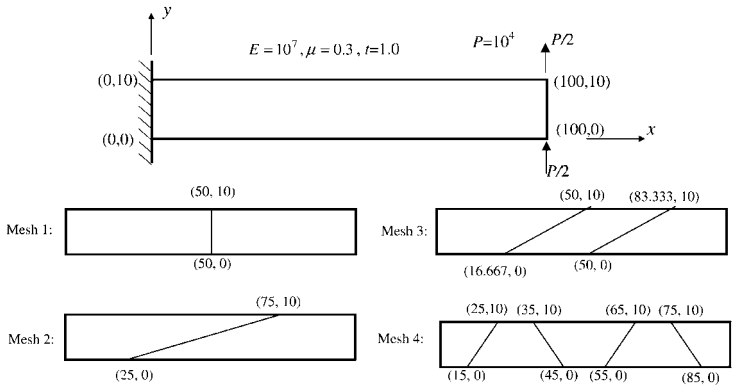

Figure 11.
Linear bending problem for a cantilever beam

		Q8	Q9	Q8α	L8	AQ8-I/II	ATF-Q8	Exact
Mesh 1	v(100,0)	3.85	3.86	3.85	3.80	3.85	*3.89*	4.03
Mesh 2	v(100,0)	0.74	3.18	3.16	3.18	3.15	*3.45*	4.03
Mesh 3	v(100,0)	2.00	3.34	3.32	3.58	3.30	*3.94*	4.03
Mesh 4	v(100,0)	3.65	3.98	3.97	3.92	3.99	*4.00*	4.03

Table XIV.
The deflection at a selected location for a linear bending problem of cantilever (Figure 11)

(4) Finally, the whole system can be rewritten in terms of element nodal displacement vector, and thus, a new hybrid element stiffness matrix is obtained.

The resulting 8-node plane element, denoted as ATF-Q8, is a new kind of finite element model that has never appeared before. Since its stress function field and boundary displacements need to be assumed independently (see Appendix), it is named as the hybrid-"stress function" element. Numerical examples show that the ATF-Q8 element possesses better performance in most cases for both displacement and stress solutions.

It is demonstrated that the new strategy for developing finite element models exhibits advantages of both analytical and discrete method. It may open a new way to promote the development of the finite element method.

References

Cen, S., Chen, X.M. and Fu, X.R. (2007), "Quadrilateral membrane element family formulated by the quadrilateral area coordinate method", *Computer Methods in Applied Mechanics and Engineering*, Vol. 196 Nos 41-44, pp. 4337-53.

Chien, W.Z. (1980), *Calculus of Variations and Finite Elements* (in Chinese), Vol. 1, Science Press, Beijing.

Cook, R.D, Malkus, D.S. and Plesha, M.E. (1989), *Concepts and Applications of Finite Element Analysis*, 3rd ed., John Wiley & Sons, New York, NY.

Hu, H.C. (1984), *Variational Principles of Theory of Elasticity with Applications*, Science Press, Beijing.

Kikuchi, F., Okabe, M. and Fujio, H. (1999), "Modification of the 8-node serendipity element", *Computer Methods in Applied Mechanics and Engineering*, Vol. 179, pp. 91-109.

Lee, N.S. and Bathe, K.J. (1993), "Effects of element distortion on the performance of isoparametric elements", *International Journal for Numerical Methods in Engineering*, Vol. 36, pp. 3553-76.

Li, C.J. and Wang, R.H. (2006), "A new 8-node quadrilateral spline finite element", *Journal of Computational and Applied Mathematics*, Vol. 195, pp. 54-65.

Li, L.X., Kunimatsu, S., Han, X.P. and Xu, S.Q. (2004), "The analysis of interpolation precision of quadrilateral elements", *Finite Elements in Analysis and Design*, Vol. 41, pp. 91-108.

Long, Y.Q. and Xu, Y. (1994), "Generalized conforming triangular membrane element with vertex rigid rotational freedom", *Finite Elements in Analysis and Design*, Vol. 17, pp. 259-71.

Long, Y.Q., Li, J.X., Long, Z.F. and Cen, S. (1999a), "Area coordinates used in quadrilateral elements", *Communications in Numerical Methods in Engineering*, Vol. 15 No. 8, pp. 533-45.

Long, Z.F., Li, J.X., Cen, S. and Long, Y.Q. (1999b), "Some basic formulae for area coordinates used in quadrilateral elements", *Communications in Numerical Methods in Engineering*, Vol. 15 No. 12, pp. 841-52.

MacNeal, R.H. and Harder, R.L. (1985), "A proposed standard set of problems to test finite element accuracy", *Finite Elements Analysis and Design*, Vol. 1 No. 1, pp. 3-20.

Ooi, E.T., Rajendran, S. and Yeo, J.H. (2008), "Remedies to rotational frame dependence and interpolation failure of US-QUAD8 element", *Communications in Numerical Methods in Engineering*, Vol. 24 No. 11, pp. 1203-17.

Rajendran, S. and Liew, K.M. (2003), "A novel unsymmetric 8-node plane element immune to mesh distortion under a quadratic displacement field", *International Journal for Numerical Methods in Engineering*, Vol. 58, pp. 1713-48.

Soh, A.K., Long, Y.Q. and Cen, S. (2000), "Development of eight-node quadrilateral membrane elements using the area coordinates method", *Computational Mechanics*, Vol. 25 No. 4, pp. 376-84.

Stricklin, J.A., Ho, W.S., Richardson. E.Q. and Haister, W.E. (1977), "On isoparametric vs linear strain triangular elements", *International Journal for Numerical Methods in Engineering*, Vol. 11, pp. 1041-43.

Washizu, K. (1982), *Variational Methods in Elasticity and Plasticity*, 3rd ed., Pergamon Press, New York, NY.

Zienkiewicz, O.C. and Taylor, R.L. (1989), *The Finite Element Method, Basic Formulation and Linear Problems*, Vol. 1, 4th ed., McGraw-Hill Book Company, London.

Appendix

The expression of **S** *in Equation (14)*

From Table I, the expression of matrix **S** in Equation (14) can be readily obtained as follows:

$$\mathbf{S}=\begin{bmatrix} 0 & 0 & 2 & 0 & 0 & 2x & 6y & 0 & 6xy & -12y^2 & 12(x^2-y^2) \\ 2 & 0 & 0 & 6x & 2y & 0 & 0 & 6xy & 0 & 12x^2 & -12(x^2-y^2) \\ 0 & -1 & 0 & 0 & -2x & -2y & 0 & -3x^2 & -3y^2 & 0 & -24xy \\ 2x(x^2-6y^2) & & & 10x^3 & & & 6x^2y & & & 10y(3x^2-2y^2) & \\ 6xy^2 & & & -10x(2x^2-3y^2) & & & -2y(6x^2-y^2) & & & 10y^3 & \\ -2y(3x^2-2y^2) & & & -30x^2y & & & 2x(2x^2-3y^2) & & & -30xy^2 & \end{bmatrix} \tag{A1}$$

The evaluation procedure of symmetrical matrix $\mathbf{M}$ *in Equation (14)*

In order to evaluate the matrix $\mathbf{M}$ by numerical integration, the Cartesian coordinates should be expressed in terms of local coordinates (isoparametric coordinates). Let:

$$x = \sum_{i=1}^{8} N_i^0(\xi,\eta)x_i, \quad y = \sum_{i=1}^{8} N_i^0(\xi,\eta)y_i, \tag{A2}$$

where (x_i, y_i) $(i = 1\text{-}8)$ are the Cartesian coordinates of the node i; $N_i^0(\xi,\eta)$ $(i = 1\text{-}8)$ are the shape functions of the standard 8-node isoparametric element Q8 and given by:

$$N_i^0 = \begin{cases} -\dfrac{1}{4}(1+\xi_i\xi)(1+\eta_i\eta)(1-\xi_i\xi-\eta_i\eta) & (i=1,2,3,4) \\ \dfrac{1}{2}(1-\xi^2)(1+\eta_i\eta) & (i=5,7) \\ \dfrac{1}{2}(1-\eta^2)(1+\xi_i\xi) & (i=6,8) \end{cases}, \tag{A3}$$

where (ξ_i, η_i) $(i = 1\text{-}8)$ are the isoparametric coordinates of the node i.

Then, after substituting Equation (A2) into Equation (A1), matrix $\mathbf{S}$ becomes:

$$\mathbf{S}(x,y) = \mathbf{S}(\xi,\eta). \tag{A4}$$

Thus, Equation (14) can be rewritten as:

$$\mathbf{M} = \int_{-1}^{1}\int_{-1}^{1} \mathbf{S}(\xi,\eta)^{\mathrm{T}}\mathbf{C}\mathbf{S}(\xi,\eta)t|\mathbf{J}|\mathrm{d}\xi\mathrm{d}\eta, \tag{A5}$$

where $|\mathbf{J}|$ is the is the Jacobian determinant, which is the same as that of the element Q8. Although an 8×8 Gauss integration scheme is theoretically needed for evaluating Equation (A5), a standard 5×5 Gauss integration scheme is found to be sufficient for the calculation of Equation (A5).

The expression of $\overline{\mathbf{N}}$ *in Equation (16)*

Assume that the displacements along each element edge are quadratic and determined by the displacements on the three nodes of each edge. Therefore, $\bar{u}$, $\bar{v}$ and corresponding matrix $\overline{\mathbf{N}}$ of each element edge can be given as follows:

$$\begin{aligned} \bar{\mathbf{u}}_{\overline{152}} &= \begin{Bmatrix} \bar{u} \\ \bar{v} \end{Bmatrix}_{\overline{152}} = \overline{\mathbf{N}}\big|_{\eta=-1}\mathbf{q}^e, \quad \bar{\mathbf{u}}_{\overline{263}} = \begin{Bmatrix} \bar{u} \\ \bar{v} \end{Bmatrix}_{\overline{263}} = \overline{\mathbf{N}}\big|_{\xi=1}\mathbf{q}^e, \\ \bar{\mathbf{u}}_{\overline{374}} &= \begin{Bmatrix} \bar{u} \\ \bar{v} \end{Bmatrix}_{\overline{374}} = \overline{\mathbf{N}}\big|_{\eta=1}\mathbf{q}^e, \quad \bar{\mathbf{u}}_{\overline{481}} = \begin{Bmatrix} \bar{u} \\ \bar{v} \end{Bmatrix}_{\overline{481}} = \overline{\mathbf{N}}\big|_{\xi=-1}\mathbf{q}^e, \end{aligned} \tag{A6}$$

where $\bar{\mathbf{u}}_{\overline{152}}$, $\bar{\mathbf{u}}_{\overline{263}}$, $\bar{\mathbf{u}}_{\overline{374}}$ and $\bar{\mathbf{u}}_{\overline{481}}$ are the boundary displacements along element edges $\overline{152}(\eta=-1), \overline{263}(\xi=1), \overline{374}(\eta=1)$ and $\overline{481}(\xi=-1)$, respectively; and

$$\overline{\mathbf{N}} = \begin{bmatrix} N_1^0 & 0 & N_2^0 & 0 & N_3^0 & 0 & N_4^0 & 0 & N_5^0 & 0 & N_6^0 & 0 & N_7^0 & 0 & N_8^0 & 0 \\ 0 & N_1^0 & 0 & N_2^0 & 0 & N_3^0 & 0 & N_4^0 & 0 & N_5^0 & 0 & N_6^0 & 0 & N_7^0 & 0 & N_8^0 \end{bmatrix}, \tag{A7}$$

in which $N_i^0(\xi,\eta)$ $(i = 1\text{-}8)$ are the shape functions of the standard 8-node isoparametric element Q8 and have been given by Equation (A3).

The evaluation procedure of matrix **H** *in Equation (16)*

The evaluation of Equation (16) should be performed along four element edges. So Equation (16) can be rewritten as:

$$\mathbf{H} = \int_{\Gamma_{12}} \mathbf{S}^{\mathrm{T}}\mathbf{L}^{\mathrm{T}}\overline{\mathbf{N}}t\mathrm{d}s + \int_{\Gamma_{23}} \mathbf{S}^{\mathrm{T}}\mathbf{L}^{\mathrm{T}}\overline{\mathbf{N}}t\mathrm{d}s + \int_{\Gamma_{34}} \mathbf{S}^{\mathrm{T}}\mathbf{L}^{\mathrm{T}}\overline{\mathbf{N}}t\mathrm{d}s + \int_{\Gamma_{41}} \mathbf{S}^{\mathrm{T}}\mathbf{L}^{\mathrm{T}}\overline{\mathbf{N}}t\mathrm{d}s, \tag{A8}$$

where Γ_{12}, Γ_{23}, Γ_{34} and Γ_{41} denote element edges $\overline{152}$, $\overline{263}$, $\overline{374}$ and $\overline{481}$, respectively.

The direction cosines of the outer normal of each element edge, l and m in Equation (5), are given by:

$$l = \frac{\mathrm{d}y}{\mathrm{d}s}, \qquad m = -\frac{\mathrm{d}x}{\mathrm{d}s}. \tag{A9}$$

Along edges $\overline{152}(\eta = -1)$ and $\overline{374}(\eta = 1)$, the relations between $\mathrm{d}s$ and $\mathrm{d}\xi$ are given by:

$$\mathrm{d}s = \left[\left(\frac{\mathrm{d}x}{\mathrm{d}\xi}\right)^2 + \left(\frac{\mathrm{d}y}{\mathrm{d}\xi}\right)^2\right]^{1/2}_{\eta=-1} \mathrm{d}\xi, \quad \mathrm{d}s = -\left[\left(\frac{\mathrm{d}x}{\mathrm{d}\xi}\right)^2 + \left(\frac{\mathrm{d}y}{\mathrm{d}\xi}\right)^2\right]^{1/2}_{\eta=1} \mathrm{d}\xi; \tag{A10}$$

and along edge $\overline{263}(\xi = 1)$ and $\overline{481}(\xi = -1)$, the relations between $\mathrm{d}s$ and $\mathrm{d}\eta$ are given by:

$$\mathrm{d}s = \left[\left(\frac{\mathrm{d}x}{\mathrm{d}\eta}\right)^2 + \left(\frac{\mathrm{d}y}{\mathrm{d}\eta}\right)^2\right]^{1/2}_{\xi=1} \mathrm{d}\eta, \quad \mathrm{d}s = -\left[\left(\frac{\mathrm{d}x}{\mathrm{d}\eta}\right)^2 + \left(\frac{\mathrm{d}y}{\mathrm{d}\eta}\right)^2\right]^{1/2}_{\xi=-1} \mathrm{d}\eta. \tag{A11}$$

Thus, substitution of Equations (A1-A4), (A6-A7), (A9-A10) into Equation (A8) yields:

$$\begin{aligned}\mathbf{H} = &\int_{-1}^{1} \mathbf{S}(\xi,-1)^{\mathrm{T}}\tilde{\mathbf{L}}\Big|_{\eta=-1}{}^{\mathrm{T}}\overline{\mathbf{N}}\big|_{\eta=-1} t\mathrm{d}\xi + \int_{-1}^{1} \mathbf{S}(1,\eta)^{\mathrm{T}}\tilde{\mathbf{L}}\Big|_{\xi=1}{}^{\mathrm{T}}\overline{\mathbf{N}}\big|_{\xi=1} t\mathrm{d}\eta \\ &- \int_{-1}^{1} \mathbf{S}(\xi,1)^{\mathrm{T}}\tilde{\mathbf{L}}\Big|_{\eta=1}{}^{\mathrm{T}}\overline{\mathbf{N}}\big|_{\eta=1} t\mathrm{d}\xi - \int_{-1}^{1} \mathbf{S}(-1,\eta)^{\mathrm{T}}\tilde{\mathbf{L}}\Big|_{\xi=-1}{}^{\mathrm{T}}\overline{\mathbf{N}}\big|_{\xi=-1} t\mathrm{d}\eta\end{aligned}, \tag{A12}$$

where

$$\tilde{\mathbf{L}}\Big|_{\eta=-1} = \begin{bmatrix} \frac{\mathrm{d}y}{\mathrm{d}\xi} & 0 & -\frac{\mathrm{d}x}{\mathrm{d}\xi} \\ 0 & -\frac{\mathrm{d}x}{\mathrm{d}\xi} & \frac{\mathrm{d}y}{\mathrm{d}\xi} \end{bmatrix}_{\eta=-1} = \begin{bmatrix} \sum_{i=1}^{8} \frac{\mathrm{d}N_i^0}{\mathrm{d}\xi} y_i & 0 & -\sum_{i=1}^{8} \frac{\mathrm{d}N_i^0}{\mathrm{d}\xi} x_i \\ 0 & -\sum_{i=1}^{8} \frac{\mathrm{d}N_i^0}{\mathrm{d}\xi} x_i & \sum_{i=1}^{8} \frac{\mathrm{d}N_i^0}{\mathrm{d}\xi} y_i \end{bmatrix}_{\eta=-1}, \tag{A13a}$$

$$\tilde{\mathbf{L}}\Big|_{\xi=1} = \begin{bmatrix} \frac{\mathrm{d}y}{\mathrm{d}\eta} & 0 & -\frac{\mathrm{d}x}{\mathrm{d}\eta} \\ 0 & -\frac{\mathrm{d}x}{\mathrm{d}\eta} & \frac{\mathrm{d}y}{\mathrm{d}\eta} \end{bmatrix}_{\xi=1} = \begin{bmatrix} \sum_{i=1}^{8} \frac{\mathrm{d}N_i^0}{\mathrm{d}\eta} y_i & 0 & -\sum_{i=1}^{8} \frac{\mathrm{d}N_i^0}{\mathrm{d}\eta} x_i \\ 0 & -\sum_{i=1}^{8} \frac{\mathrm{d}N_i^0}{\mathrm{d}\eta} x_i & \sum_{i=1}^{8} \frac{\mathrm{d}N_i^0}{\mathrm{d}\eta} y_i \end{bmatrix}_{\xi=1}, \tag{A13b}$$

$$\tilde{\mathbf{L}}\Big|_{\eta=1} = \begin{bmatrix} \dfrac{\mathrm{d}y}{\mathrm{d}\xi} & 0 & -\dfrac{\mathrm{d}x}{\mathrm{d}\xi} \\ 0 & -\dfrac{\mathrm{d}x}{\mathrm{d}\xi} & \dfrac{\mathrm{d}y}{\mathrm{d}\xi} \end{bmatrix}_{\eta=1} = \begin{bmatrix} \sum_{i=1}^{8} \dfrac{\mathrm{d}N_i^0}{\mathrm{d}\xi} y_i & 0 & -\sum_{i=1}^{8} \dfrac{\mathrm{d}N_i^0}{\mathrm{d}\xi} x_i \\ 0 & -\sum_{i=1}^{8} \dfrac{\mathrm{d}N_i^0}{\mathrm{d}\xi} x_i & \sum_{i=1}^{8} \dfrac{\mathrm{d}N_i^0}{\mathrm{d}\xi} y_i \end{bmatrix}_{\eta=1}, \quad \text{(A13c)}$$

$$\tilde{\mathbf{L}}\Big|_{\xi=-1} = \begin{bmatrix} \dfrac{\mathrm{d}y}{\mathrm{d}\eta} & 0 & -\dfrac{\mathrm{d}x}{\mathrm{d}\eta} \\ 0 & -\dfrac{\mathrm{d}x}{\mathrm{d}\eta} & \dfrac{\mathrm{d}y}{\mathrm{d}\eta} \end{bmatrix}_{\xi=-1} = \begin{bmatrix} \sum_{i=1}^{8} \dfrac{\mathrm{d}N_i^0}{\mathrm{d}\eta} y_i & 0 & -\sum_{i=1}^{8} \dfrac{\mathrm{d}N_i^0}{\mathrm{d}\eta} x_i \\ 0 & -\sum_{i=1}^{8} \dfrac{\mathrm{d}N_i^0}{\mathrm{d}\eta} x_i & \sum_{i=1}^{8} \dfrac{\mathrm{d}N_i^0}{\mathrm{d}\eta} y_i \end{bmatrix}_{\xi=-1}. \quad \text{(A13d)}$$

Five Gauss integration points are theoretically needed for evaluating Equation (A12).

Corresponding author
Song Cen can be contacted at: censong@tsinghua.edu.cn